

Bubbles in ^{34}Si and ^{22}O ?

M. Grasso,¹ L. Gaudefroy,² E. Khan,¹ T. Nikšić,³ J. Piekarewicz,⁴ O. Sorlin,⁵ N. Van Giai,¹ and D. Vretenar³

¹*Institut de Physique Nucléaire, Université Paris-Sud, IN2P3-CNRS, F-91406 Orsay Cedex, France*

²*CEA/DAM Ile de France, Service de Physique Nucléaire, Bruyère-le-Châtel, F-91297 Arpajon Cedex, France*

³*Physics Department, Faculty of Science, Zagreb University, 10000 Zagreb, Croatia*

⁴*Florida State University, Tallahassee, Florida 32306, USA*

⁵*Grand Accélérateur National d'Ions Lourds (GANIL), CEA/DSM-CNRS-IN2P3, Bd Henri Becquerel, BP 55027, F-14076 Caen Cedex 5, France*

Bubble nuclei are characterized by a depletion of their central density. Their existence is examined within three different theoretical frameworks: the shell model as well as non-relativistic and relativistic microscopic mean-field approaches. We propose ^{34}Si and ^{22}O as possible candidates for proton and neutron bubble nuclei, respectively. In the case of ^{22}O , we observe a significant model dependence, thereby calling into question the bubble structure of ^{22}O . In contrast, an overall agreement among the models is obtained for ^{34}Si . Indeed, all models predict a central proton density depletion of about 40%. This result provides strong evidence in favor of a proton bubble in ^{34}Si .

PACS numbers: 21.10.Ft, 21.10.Re, 21.60.Jz, 25.30.Bf, 25.70.De

I. INTRODUCTION

The “bubble” structure of atomic nuclei is characterized by a depleted central density. Although it is somewhat unexpected that a “hole” can be made in a nuclear system where nuclear forces generate a saturation density ($\rho_0 \sim 0.16 \text{ fm}^{-3}$), this phenomenon has been discussed for many decades. Indeed, the possibility of bubble nuclei started with the pioneering work of Wilson in the 40s [1] who studied the low-energy excitations of a thin spherical shell, up to the first microscopic calculations of Campi and Sprung in the 70s [2]. More recently, bubbles have been discussed in superheavy and hyperheavy nuclei [3, 4]. The promise of producing more exotic nuclei with the new generation of RIB facilities has revived the interest in this subject.

Due to the absence of a centrifugal barrier, s -orbitals have radial distributions peaked in the interior of the nucleus, with their corresponding wave function extending further into the surface depending on the number of nodes. In contrast, orbitals with non-zero angular momenta are suppressed in the nuclear interior and do not contribute to the central density. Therefore, any vacancy of s -orbitals is expected to produce a depletion of the central density. By using electron scattering from ^{206}Pb and ^{205}Tl up to large momentum transfers, the radial distribution of the $3s$ proton orbital was experimentally mapped and shown to closely resemble the one predicted by an independent particle model. The agreement extends from the center of the ^{206}Pb nucleus all the way to the surface and reproduces accurately the nodal structure of the wave function [5, 6]. Differences in the charge density between ^{206}Pb and ^{205}Tl revealed that about 80% of the proton removal strength came from the $3s$ state, thereby leading to a significant depletion of the proton density in the nuclear interior. Specifically, the depletion

fraction, defined as

$$F \equiv \frac{\rho_{\text{max}} - \rho_c}{\rho_{\text{max}}}, \quad (1)$$

amounts to $F = 11(2)\%$. Note that here ρ_c and ρ_{max} represent the values of the central and maximum charge density in ^{205}Tl , respectively. Yet the small energy difference between the $3s_{1/2}$ and the $2d_{3/2}$ proton orbitals plus the coupling of the $3s_{1/2}$ proton to collective excitations in ^{206}Pb , yield a proton hole strength in ^{205}Tl that is shared among the $3s_{1/2}$ and $2d_{3/2}$ orbitals, with the former carrying about 70% of the strength and the latter the remaining 30%. Consequently, the central depletion in ^{205}Tl relative to ^{206}Pb is not as large as if the full hole strength would have been carried by the $3s$ orbital. Using similar arguments, the depletion at the center of ^{204}Hg is not expected to be very large, as the two-proton hole strength will be again shared among the $3s_{1/2}$ and $2d_{3/2}$ orbitals. Therefore, the search for the best bubble candidates should be oriented towards nuclei with an s orbital well separated from its nearby single-particle states and where correlations are weak. This latter feature arises mainly for nuclei located at major shell closures.

Recently, the formation of a proton bubble due to the depletion of the $2s_{1/2}$ orbital was investigated in ^{46}Ar [7, 8] and in the very neutron-rich Ar isotopes [8]. In ^{46}Ar the proton $2s_{1/2}$ and $1d_{3/2}$ orbitals are almost degenerate. Thus, as in the case of ^{206}Pb , pairing correlations will lead to a significant occupancy of the $2s_{1/2}$ orbital [9], thus weakening the bubble effect. This weakening will continue to hold for any $N = 28$ isotone between $Z = 20$ and $Z = 14$ as long as the $2s_{1/2}$ and $1d_{3/2}$ orbitals remain degenerate, as shown for instance in Fig. 3 of Ref. [10]. For very neutron-rich Ar isotopes, such as ^{68}Ar , the $s_{1/2}$ proton orbital is predicted to move significantly above the $d_{3/2}$ state, hindering the role of pairing correlations [8, 11]. Unfortunately, the production of this exotic nucleus is far beyond the present and

near-future capabilities of RIB facilities.

A more suitable region of the chart of the nuclides to search for a proton bubble is that of the $N = 20$ isotones. Between $Z = 20$ and $Z = 16$ the $s_{1/2}$ orbital is located about 6.5 MeV above the $d_{5/2}$ orbital and about 2.5 MeV below the $d_{3/2}$ orbital, thereby forming two subshell closures at $Z = 14$ and $Z = 16$, respectively [12]. In addition, the $N = 20$ shell closure is rigid enough to hinder significant coupling to collective states. Assuming a sequential filling of proton orbitals, the $2s_{1/2}$ orbital should be completely empty in ^{34}Si while fully filled in ^{36}S . This may lead to an important change in the proton density distribution between ^{36}S and ^{34}Si making ^{34}Si an excellent candidate for a bubble nucleus. Concomitantly, both Skyrme and Gogny Hartree-Fock-Bogoliubov models predict a spherical shape for ^{34}Si [13, 14]. Other possible candidates in the Si-isotopic chain, such as ^{28}Si and ^{42}Si , are not optimal as they are deformed [15, 16]. For these nuclei several correlations hinder the development of a bubble. The mirror system of the (^{36}S , ^{34}Si) system, (^{36}Ca , ^{34}Ca), could not be studied at present because the ^{34}Ca nucleus has so far not been observed.

A neutron bubble may be found in the oxygen chain, where large $N = 14$ (between $d_{5/2}$ and $s_{1/2}$) and $N = 16$ (between $s_{1/2}$ and $d_{3/2}$) subshell gaps of about 4.2 MeV [17, 18] and 4 MeV [19], respectively, have been determined. Combined to the large proton gap at $Z = 8$, the ^{22}O [17, 20, 21] and ^{24}O [18, 19, 22] therefore behave as doubly magic nuclei. In this case the change in the occupancy of the $2s_{1/2}$ neutron orbital will occur between ^{22}O and ^{24}O , making ^{22}O a good candidate for a neutron bubble nucleus.

The present article aims at determining whether ^{34}Si and ^{22}O could be considered as good proton and neutron bubble nuclei, respectively. Various theoretical approaches will be employed to test the robustness of the results. In Sec. II these nuclei are analyzed in terms of shell-model calculations so that occupancies of the proton and neutron orbitals may be determined. In Sec. III we start by addressing (in III-A) the role of pairing correlations in mean field approaches, followed then with results on nucleon density profiles obtained from: (i) non-relativistic Hartree-Fock (HF) and Hartree-Fock-Bogoliubov (HFB) (in III-B) and (ii) relativistic mean field (RMF) and relativistic Hartree-Bogoliubov (RHB) (in III-C) microscopic calculations. Comparison to experimental data will be made whenever possible. Conclusions are drawn in Sec. IV.

II. SHELL-MODEL PREDICTIONS

The occurrence of bubbles in nuclei, as previously defined, is directly linked to the occupancy of $s_{1/2}$ orbitals. For both bubble candidates under study in this article, ^{22}O and ^{34}Si , experimental values for the occupancies are not yet available. Thus, we rely hereafter on Shell Model (SM) calculations that are known to give reli-

TABLE I: Ground state occupation numbers of neutron orbitals obtained in the SM framework for ^{24}O and ^{22}O .

Orbital	^{24}O	^{22}O
$\nu 1d_{5/2}$	5.75	5.38
$\nu 2s_{1/2}$	1.89	0.34
$\nu 1d_{3/2}$	0.36	0.28

able estimates in neutron-rich nuclei occupying the *sdpf* shells [25].

Shell-model calculations have been performed with the ANTOINE code [23, 24] using the SDPF-NR interaction [25]. The full *sd* valence space was considered for both proton and neutron excitations for each nucleus under consideration. Moreover, in the calculations for ^{36}S and ^{34}Si , $4p4h$ neutron excitations were allowed from the $\nu d_{3/2}$ to the $\nu f_{7/2}$ orbitals.

A. Neutron Bubble: ^{24}O and ^{22}O

The mean occupation numbers of neutron orbitals deduced from SM calculations are reported in Table I. Contrary to naive expectations, the mean number of neutrons removed from the $\nu s_{1/2}$ orbital while moving from ^{24}O to ^{22}O amounts to only 1.55 (or 78% in fraction of shell occupancy). The remaining neutron strength is removed from the $\nu d_{5/2}$ orbital (0.37 or 18%) and the $\nu d_{3/2}$ orbital (0.08 or 4%). These numbers suggest that the depletion of the neutron density in the nuclear interior of ^{22}O relative to ^{24}O may not be as large as required for the formation of a bubble structure. To quantify the size of the neutron hole the radial dependence of the neutron wave functions in $^{22,24}\text{O}$ have been calculated using a standard Woods-Saxon potential [26], the parameters of which are as follows: $V_0 = -50$ MeV, $a = 0.65$ fm and $r_0 = 1.25$ fm. The neutron densities displayed in Fig. 1 are the sum of the squared wave functions calculated with the Woods-Saxon potential (without spin-orbit term) weighted by the occupation numbers obtained within the SM framework. The orbitals occupied by the core neutrons (namely, the $1\nu s_{1/2}$, $1\nu p_{3/2}$ and $1\nu p_{1/2}$ orbitals) are assumed to be completely filled. The figure shows the variation of the neutron density between ^{24}O and ^{22}O . In particular, the predicted depletion fraction, as defined in Eq. (1), is found to be $F = 25\%$. As will be shown in the following section, the depletion in ^{22}O is considerably smaller than in ^{34}Si . One notices that in the lighter Oxygen isotopes this depletion factor is not expected to increase as the neutron $1\nu d_{5/2}$ orbital is depleted in concert, thus lowering the maximum value of the density around the surface of the nucleus. It follows that the relative difference of the density in the vicinity of the surface and at the interior of the nucleus is also reduced.

TABLE II: Same as Table I for ^{36}S and ^{34}Si . The third column shows the experimental occupancies obtained in Ref. [27] for ^{36}S .

Orbital	^{36}S	^{34}Si	^{36}S (Ref. [27])
$\pi 1d_{5/2}$	5.85	5.75	6.1(12)
$\pi 2s_{1/2}$	1.88	0.09	1.63(32)
$\pi 1d_{3/2}$	0.27	0.16	0.31(6)

B. Proton Bubble: ^{36}S and ^{34}Si

The mean occupation numbers of the proton $1d_{3/2}$, $2s_{1/2}$ and $1d_{5/2}$ orbitals in ^{36}S have been obtained from the $^{36}\text{S}(d, ^3\text{He})^{35}\text{P}$ experiment done by S. Khan and collaborators [27]. The sum of the deduced spectroscopic factors from the proton pickup reaction from the whole sd states amounts to $\sum C^2S \approx 7.9$. Within the 20% uncertainties of the method, this exhausts the complete spectroscopic shell model strength of $\sum C^2S = 8$. Experimental occupancies of the $2s_{1/2}$ and $1d_{3/2}$ orbitals as reported in Table II are 1.63 and 0.31, respectively. Note that the small occupancy of the $1d_{3/2}$ state is due to correlations.

As already mentioned, $4p4h$ neutron excitations from the $\nu d_{3/2}$ to the $\nu f_{7/2}$ orbitals have been allowed in the present SM calculations. This provides an estimate of the contribution of neutron cross-shell excitations (across the $N = 20$ shell closure). Such contributions are found to be negligible ($< 2\%$). Indeed, both ^{36}S and ^{34}Si ground states have quasi pure single-particle wave functions. For ^{34}Si [^{36}S], the $(\pi d_{5/2})^6(\nu sd)^{12}$ [$(\pi d_{5/2})^6(\pi s_{1/2})^2(\nu sd)^{12}$] configuration represents about 87% [85%] of the ground state wave function. The mean occupation numbers for the proton orbitals deduced from the present SM calculations are reported in Table II. The agreement with the experimental values for ^{36}S is very good, lending confi-

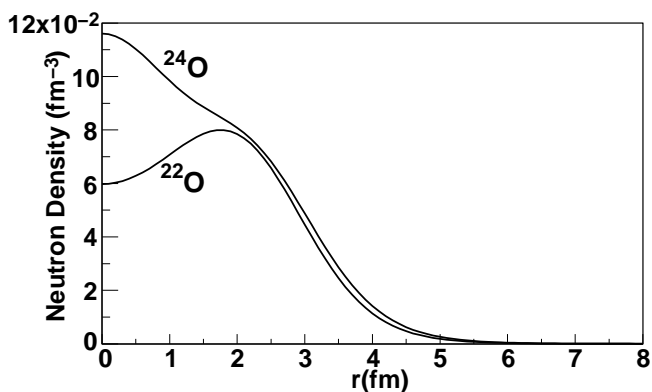


FIG. 1: Neutron density of ^{24}O and ^{22}O obtained using the occupation numbers of neutron orbitals resulting from SM calculations and radial wave functions obtained with a Woods-Saxon potential (see text).

dence to the SM predictions for ^{34}Si . The study of the $^{34}\text{Si}(d, ^3\text{He})^{33}\text{Al}$ reaction channel should be used in the future to determine if the occupancy of the $2s_{1/2}$ proton orbital has indeed dropped to nearly zero in ^{34}Si .

The proton fraction removed from the $2\pi s_{1/2}$ orbital, while moving from ^{36}S to ^{34}Si , is significantly larger than the corresponding case in the Oxygen isotopes. Moreover, a larger mean occupation number of the $d_{5/2}$ orbitals is predicted in ^{34}Si as compared to ^{22}O . Both of these effects combined to explain the larger depletion in the nuclear interior of ^{34}Si , as displayed in Fig. 2. The densities presented in this figure have been obtained in the same way as for $^{24,22}\text{O}$. The depletion factor in ^{34}Si is found to be $F = 43\%$, significantly larger than in ^{22}O . Thus, we conclude that within this approach, ^{34}Si is a good candidate for a proton bubble. We are aware that the nucleon densities reported above may not be as reliable as the mean occupation numbers extracted from the SM code. The self-consistent microscopic treatment presented in the following sections is more appropriate to provide radial densities.

III. MEAN FIELD CALCULATIONS

Self-consistent mean-field approaches enable to determine microscopically the density distributions of nuclei. Nucleon occupation factors may also be determined by taking pairing correlations into account. As a first step in describing the density distributions, one must determine the role of pairing correlations, if any, on the development of proton and neutron bubbles in ^{34}Si and ^{22}O nuclei, respectively.

A. Pairing effects

As already alluded to in the Introduction, ^{22}O is expected to behave almost as a doubly-magic nucleus, being that the $N = 14$ sub-shell closure has been experimentally determined. However, as shown in the previous

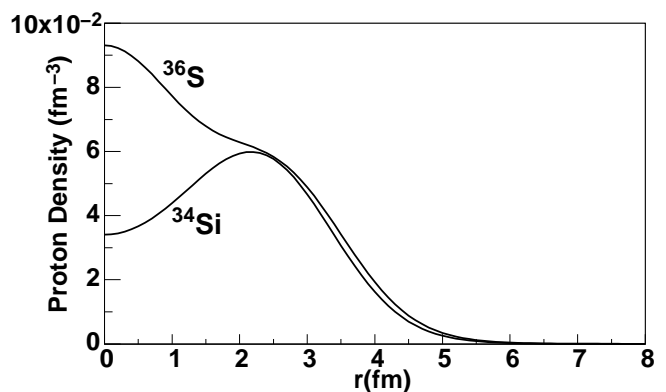


FIG. 2: Same as Fig. 1 for proton densities in ^{36}S and ^{34}Si .

section, SM calculations predict a 17% occupancy of the $2s$ neutron state, suggesting that pairing correlations are likely to have some effect on this nucleus. The effect of pairing correlations on the neutron density profile of ^{22}O will be shown in the following subsections for both the non-relativistic and the relativistic mean-field cases.

Let us now consider the case of ^{34}Si . To start, we discuss the role of pairing in the non-relativistic case. In this case pairing correlations can be modeled in the Skyrme-Hartree-Fock-Bogoliubov (Skyrme-HFB) framework by adopting the following zero-range density dependent pairing interaction:

$$V_{pair} = V_0 \left[1 - \eta \left(\frac{\rho(r)}{\rho_0} \right)^\alpha \right] \delta(\mathbf{r}_1 - \mathbf{r}_2), \quad (2)$$

with $\eta = 0.5$ (mixed surface-volume interaction), $\alpha = 1$ and $\rho_0 = 0.16 \text{ fm}^{-3}$. In the particle-hole channel, we employ the SLy4 Skyrme parametrization that is well suited to describe neutron-rich nuclei.

We fix the parameter V_0 in Eq. (2) to reproduce the two-proton separation energy in ^{34}Si . Note that the two-proton separation energy is defined as:

$$S_{2p} = E(N, Z) - E(N, Z - 2), \quad (3)$$

where $E(N, Z)$ is the total binding energy of the (N, Z) nucleus. It should be noted that the experimental value of 33.74 MeV is already reasonably well reproduced without pairing: the HF value is equal to 35.19 MeV. Moreover the HFB calculations—which include the pairing interaction—yield negligible corrections, as $Z = 14$ is predicted by the HFB approach to be a robust sub-shell closure in agreement with the shell model spectroscopic factors (see Table II where the SM occupation of the s state is only 4.5%). Thus, we can safely perform the analysis of this nucleus with the HF model, where pairing is absent. Note that the above results will be confirmed in Subsec. C within the relativistic approach where pairing effects are also found to collapse in the case of ^{34}Si .

B. Non-relativistic mean field approach

In this Subsection both ^{22}O and ^{34}Si are analyzed as possible candidates for bubbles nuclei. Figure 3 displays neutron density profiles in ^{22}O (full line) and ^{24}O (dashed line) calculated self-consistently within the SLy4-HF approach. In the case of ^{24}O the neutron single-particle state $2s_{1/2}$ is assumed to be fully occupied. The depletion of the central density in ^{22}O relative to ^{24}O is clearly visible. However, the bubble profile is not evident: since the central neutron density in ^{24}O is strongly enhanced, the depletion in ^{22}O does not lead to the development of a significant central hole. The central depletion fraction F is $\sim 13\%$, much weaker than the SM result. As one switches on pairing and chooses the same parameters as in Ref. [28] for the pairing interaction, the central hole is seen to be completely washed out (see the dotted line

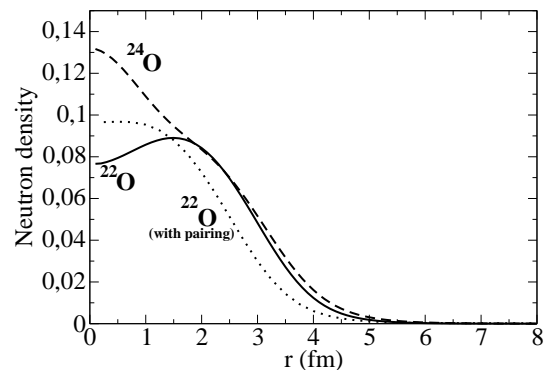


FIG. 3: HF neutron densities (in units of fm^{-3}) of ^{22}O (full line) and ^{24}O (dashed line) calculated with the Skyrme interaction SLy4. The dotted line represents the SLy4-HFB neutron density of ^{22}O .

in Fig. 3). Note that the density profile of ^{24}O remains unchanged when pairing is switched on.

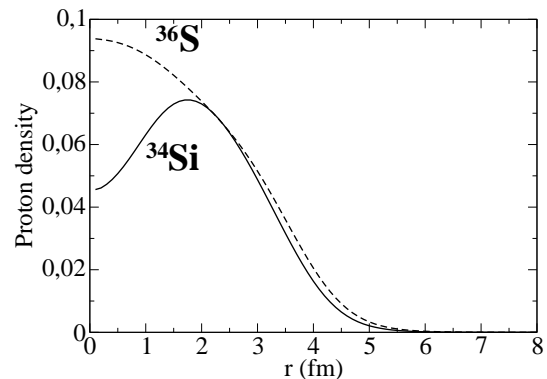


FIG. 4: HF proton densities (in units of fm^{-3}) of ^{36}S (dashed line) and ^{34}Si (solid line) calculated with the Skyrme interaction SLy4.

The SLy4-HF proton density profiles calculated in ^{34}Si and ^{36}S (where the s state is fully occupied) are shown in Fig. 4. One observes that the bubble is much more prominent in this case than in ^{22}O . The depletion fraction F is $\sim 38\%$ and in very good agreement with the SM value. We should mention that pairing is expected to modify the density profile of ^{36}S , but this is not relevant here since this density is plotted only to better appreciate the central hole in ^{34}Si . By comparing the HF proton density in ^{34}Si with the HF neutron density in ^{22}O , one observes that the central value in ^{34}Si is much lower than in ^{22}O . The contribution to the central value of the density is entirely due to the first s wave function, i.e. the $1s$. The difference between the two central values may be related to the presence of a neutron excess at the surface of ^{34}Si . The effect of this neutron-skin on the proton $1s_{1/2}$ wave function is to attract and push it towards the surface, thereby lowering its value at the center. This

can be observed in Fig. 5 where the neutron (proton) $1s$ contribution to the HF density is plotted for ^{22}O (^{34}Si).

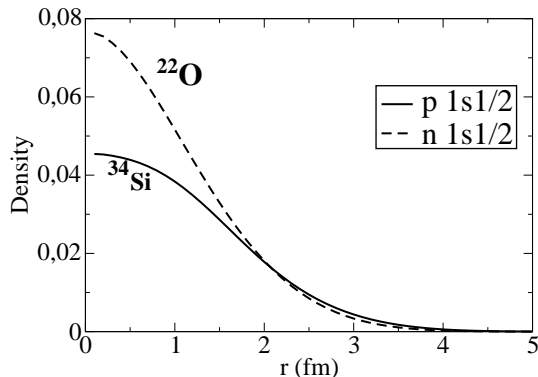


FIG. 5: Neutron (proton) $1s$ contributions to the density (in units of fm^{-3}) for ^{22}O (^{34}Si).

C. Relativistic mean field approach

As in the previous section, calculations are performed for the two Oxygen isotopes ^{22}O and ^{24}O as well as for the two $N = 20$ isotones ^{34}Si and ^{36}S , but now using a relativistic mean field (RMF) approach. Pairing effects are evaluated within the relativistic Hartree-Bogoliubov (RHB) model. In one particular realization of the relativistic formalism the dynamics of the system is dictated by an interacting Lagrangian density of the following form:

$$\begin{aligned} \mathcal{L}_{\text{int}} = & \bar{\psi} \left[g_s \phi - \left(g_v V_\mu + \frac{g_\rho}{2} \tau \cdot \mathbf{b}_\mu + \frac{e}{2} (1 + \tau_3) A_\mu \right) \gamma^\mu \right] \psi \\ & - \frac{\kappa}{3!} (g_s \phi)^3 - \frac{\lambda}{4!} (g_s \phi)^4 + \frac{\zeta}{4!} (g_v^2 V_\mu V^\mu)^2 \\ & + \Lambda_v (g_\rho^2 \mathbf{b}_\mu \cdot \mathbf{b}^\mu) (g_v^2 V_\mu V^\mu). \end{aligned} \quad (4)$$

where ψ represents an isodoublet nucleon field interacting via the exchange of two isoscalar mesons — a scalar (ϕ) and a vector (V^μ) — one isovector meson (b^μ), and the photon (A^μ) [29, 30]. In addition to meson-nucleon interactions, the Lagrangian density is supplemented by non-linear meson interactions with coupling constants denoted by κ , λ , ζ , and Λ_v that are responsible for a softening of the nuclear-matter equation of state, both for symmetric and pure-neutron matter. For the RMF case we consider two parametrizations: the very successful NL3 parameter set [31, 32] and a more recent set known as FSUGold [33]. The main difference between these two models lies in the prediction of the density dependence of the symmetry energy. This difference manifests itself in significantly larger neutron skins for NL3 than for FSUGold [33]. Neutron skins for the two isotones of interest in the present work, alongside other ground-state properties, have been listed in Table III for ^{34}Si and ^{36}S .

Model	$B/A(\text{MeV})$	$R_{ch}(\text{fm})$	$R_n - R_p(\text{fm})$
NL3	8.36	3.13	0.25
FSUGold	8.28	3.13	0.21
Experiment	8.34	—	—
NL3	8.50	3.26	0.12
FSUGold	8.42	3.26	0.09
Experiment	8.58	3.28	—

TABLE III: Binding energy per nucleon, charge radii, and neutron skin thickness for ^{34}Si (upper block) and ^{36}S (lower block) as predicted by the two RMF models used in this work. When available, experimental data is provided for comparison.

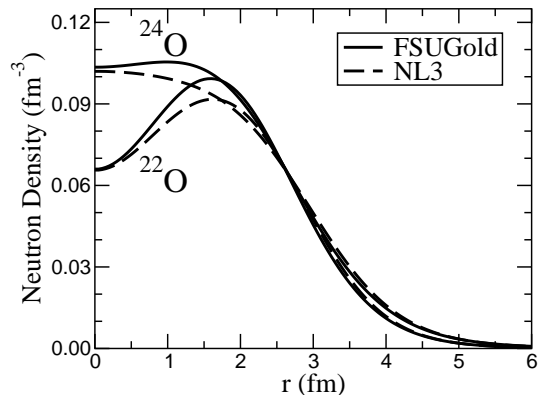


FIG. 6: RMF neutron densities of ^{22}O and ^{24}O calculated with the two RMF models described in the text.

RMF neutron densities for the two neutron-rich isotopes ^{22}O and ^{24}O are displayed in Fig. 6. Whereas the RMF results show a mild model dependence, differences between the relativistic and non-relativistic models are significant. Indeed, in contrast to the non-relativistic case, the relativistic results display no enhancement of the central neutron density in ^{24}O . Moreover, the removal of both $2s_{1/2}$ neutrons from ^{24}O yields a strong depletion of the interior neutron density in ^{22}O . As a result, a central depletion fraction of $F = 34\%$ (28%) is predicted for ^{22}O by the FSUGold(NL3) model. These values are significantly larger than the 13% depletion fraction obtained with the SLy4-HF parametrization, but close to the SM expectations. It may be interesting to elucidate the source behind this discrepancy which might be related to the saturation mechanism in RMF and HF calculations.

In the case of the larger nuclei ^{34}Si and ^{36}S one observes, now in agreement with the non-relativistic and the SM cases, how the proton density of ^{34}Si is significantly depleted in the nuclear interior and how the proton bubble disappears as soon as the $2s_{1/2}$ proton orbital is filled in ^{36}S (see Fig. 7). Indeed, not only is the central density in ^{34}Si strongly depleted, but the central density in ^{36}S

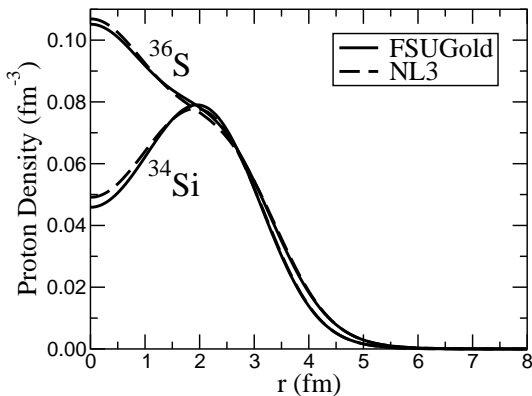


FIG. 7: RMF proton densities of ^{36}S and ^{34}Si calculated with the two RMF models described in the text.

also appears to be get greatly enhanced. This behavior results in central depletion factors for ^{34}Si of $F = 42\%$ and $F = 37\%$ for the FSUGold and NL3 parameter sets, respectively. These numbers are in good agreement with the non-relativistic prediction of $F \sim 38\%$ and SM of $\sim 43\%$.

Let us quantify now the effects of pairing correlations within the RHB model. A medium dependence for a relativistic mean-field interaction can either be introduced by including non-linear meson self-interaction terms in the Lagrangian, as in the case of NL3 and FSUGold, or by assuming an explicit density dependence for the meson-nucleon couplings. This is the case of the DD-ME2 model [34] that we adopt to perform RHB calculations. The couplings of the σ -meson and ω -meson to the nucleon are assumed to be of the form:

$$g_i(\rho) = g_i(\rho_{sat})f_i(x) \quad \text{for } i = \sigma, \omega, \quad (5)$$

where

$$f_i(x) = a_i \frac{1 + b_i(x + d_i)^2}{1 + c_i(x + d_i)^2} \quad (6)$$

is a function of $x = \rho/\rho_{sat}$, and ρ_{sat} denotes the nucleon density at saturation in symmetric nuclear matter. Constraints at nuclear matter saturation density and at zero density are used to reduce the number of independent parameters in Eq. (6) to three. Three additional parameters in the isoscalar channel are $g_\sigma(\rho_{sat})$, $g_\omega(\rho_{sat})$, and m_σ —the mass of the phenomenological σ meson. For the ρ meson coupling the functional form of the density dependence is suggested by Dirac-Brueckner calculations of asymmetric nuclear matter:

$$g_\rho(\rho) = g_\rho(\rho_{sat}) \exp[-a_\rho(x - 1)], \quad (7)$$

and the isovector channel is parametrized by $g_\rho(\rho_{sat})$ and a_ρ . Bare values are used for the masses of the ω and ρ mesons: $m_\omega = 783$ MeV and $m_\rho = 763$ MeV. DD-ME2

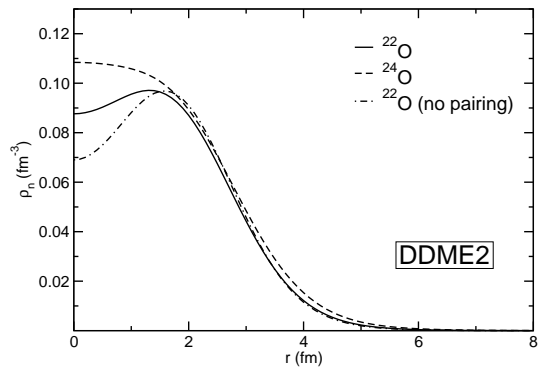


FIG. 8: Neutron density profiles of ^{22}O and ^{24}O calculated in the RHB model with the density-dependent RMF interaction DD-ME2, and Gogny pairing.

is determined by eight independent parameters, adjusted to the properties of symmetric and asymmetric nuclear matter, binding energies, charge radii, and neutron radii of spherical nuclei [34]. The interaction has been tested in the calculation of ground state properties of large set of spherical and deformed nuclei. When used in the relativistic RPA, DD-ME2 reproduces with high accuracy data on isoscalar and isovector collective excitations [34?].

In Figs. 8 and 9 we display the neutron (proton) density profiles for $^{22,24}\text{O}$, ^{34}Si and ^{36}S , calculated in RHB model [35] with the DD-ME2 effective interaction in the particle-hole channel, and with the Gogny interaction [36] in the pairing channel

$$V^{PP}(1,2) = \sum_{i=1,2} e^{-((\mathbf{r}_1 - \mathbf{r}_2)/\mu_i)^2} (W_i + B_i P^\sigma - H_i P^\tau - M_i P^\sigma P^\tau), \quad (8)$$

with the set D1S [37] for the parameters μ_i , W_i , B_i , H_i , and M_i ($i = 1, 2$).

For ^{24}O and ^{34}Si the RHB calculation with the DD-ME2 interaction predicts neutron and proton density profiles similar to those calculated with NL3 and FSUGold. Because of the large gaps: between $\nu s_{1/2}$ and $\nu d_{3/2}$ (> 4 MeV) in ^{24}O , and between $\pi d_{5/2}$ and $\pi s_{1/2}$ (> 6 MeV) in ^{34}Si , we find a pairing collapse in these nuclei, in agreement with non-relativistic predictions. On the other hand, the inclusion of pairing correlations has a pronounced effect on the neutron and proton density profiles in ^{22}O and ^{36}S , respectively. When pairing is set to zero (dash-dot curves in Figs. 8 and 9) the $\nu s_{1/2}$ orbital is empty in ^{22}O , and the $\pi s_{1/2}$ orbital is fully occupied in ^{36}S . The resulting DD-ME2 density profiles are again very similar to those calculated with the two other RMF interactions. However, the pairing interaction in the RHB model calculation modifies the occupancy of the two $2s_{1/2}$ orbitals, thus reducing the pronounced bubble

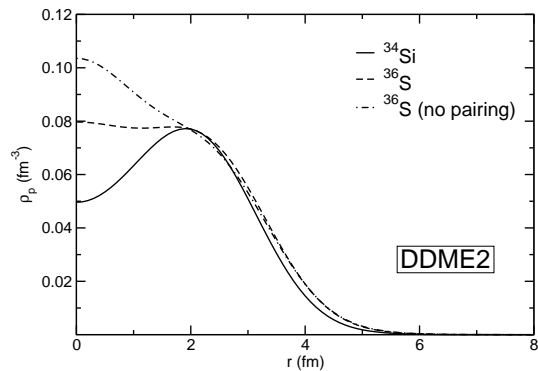


FIG. 9: Proton densities of ^{36}S and ^{34}Si calculated in the RHB model with the DD-ME2 interaction plus Gogny D1S pairing.

Nucleus	SM	SLy4	SLy4	NL3	FSUGold	DDME2	DDME2
		HF	HFB	RMF	RMF	RMF	RHB
^{22}O	25%	13%	0	28%	34%	29%	10%
^{34}Si	43%	38%	38%	37%	42%	36%	36%

TABLE IV: Central fraction of depletion F

in the neutron density of ^{22}O , as well as the prominent cusp in the proton density of ^{36}S .

In the DD-ME2 model the F values are found equal to 29%, 10% and 36% for ^{22}O (without pairing), ^{22}O (with pairing) and ^{34}Si (same result with and without pairing), respectively.

IV. SUMMARY AND CONCLUSIONS

The occurrence of proton and neutron bubbles in ^{34}Si and ^{22}O , respectively, has been investigated using three

different theoretical approaches: (i) the shell model, (ii) the Skyrme mean-field model, and (iii) the relativistic mean-field model. This occurrence can be quantified by the values of the depletion fraction F which we have evaluated in these different approaches and which are summarized in table IV.

For the ^{22}O nucleus a significant model dependence has been found. Moreover, in both non-relativistic and relativistic cases, pairing correlations have been shown to weaken the bubble phenomenon. In contrast, for ^{34}Si an overall agreement exists: a central depletion fraction of $\sim 40\%$ is predicted by all the models. Although not discussed here, the presence of this proton bubble is expected to induce quenching of the spin-orbit splitting of the neutron $2p$ orbitals in ^{34}Si (see Refs. [7, 9] for details).

These robust results indicate that ^{34}Si is a good candidate for a bubble density profile. The measurement of the charge density in ^{34}Si could be undertaken, for instance, by electron scattering in a exotic beam collider, such as EXL in FAIR and RIBF in Riken. The bubble impact on the momentum distribution in these experiment has been investigated in Ref. [8]. The study of ^{34}Si , either by high energy proton scattering (to focus on the matter distribution) or by direct reactions (to yield the spectroscopic factors and the low-energy excitation spectrum) is already feasible [8]. For the transfer reaction, the $^{34}\text{Si}(d, ^3\text{He})^{33}\text{Al}$ reaction channel should be used to determine if the occupancy of the $2s_{1/2}$ proton orbit has dropped to nearly zero in ^{34}Si . This would confirm the SM predictions shown in Sec. II, while providing strong evidence in favor of a strongly depleted central density in ^{34}Si .

Acknowledgments The authors thank K. Yoshida for valuable discussions. The research of J.P. is supported in part by the United States DOE grant DE-FD05-92ER40750.

-
- [1] H.A. Wilson, *Phys. Rev.* **69** (1946) 538.
[2] X. Campi, D.W.L. Sprung *Phys. Lett.* **B46** (1973) 291.
[3] M. Bender, K. Rutz, P.-G. Reinhard, J.A. Maruhn, W. Greiner, *Phys. Rev.* **C60** (2003) 55.
[4] J. Dechargé, J.-F. Berger, M. Girod, K. Dietrich, *Nucl. Phys.* **A716** (2003) 55.
[5] J.M. Cavedon et al., *Phys. Rev. Lett.* **49** (1982) 978.
[6] V.R. Pandharipande, I. Sick, and P.K.A. deWitt Huberts, *Rev. Mod. Phys.* **69** (1997) 981.
[7] B.G. Todd-Rutel, J. Piekarewicz, P.D. Cottle, *Phys. Rev.* **C69** (2004) 021301(R)
[8] E. Khan, M. Grasso, J. Margueron, N. Van Giai, *Nucl. Phys.* **A800** (2008) 37.
[9] L. Gaudefroy et al., *Phys. Rev. Lett.* **99** (2007) 099202.
[10] A. Gade et al., *Phys. Rev.* **C 74** (2006) 034322.
[11] M. Grasso, Z.Y. Ma, E. Khan, J. Margueron, N. Van Giai, *Phys. Rev.* **C76** (2007) 044319.
[12] O. Sorlin and M.G. Porquet, *Prog. Part. Nucl. Phys.* **61** (2008) 602.
[13] K. Yoshida, Private communication
[14] S. Hilaire, M. Girod, http://www-phynu.cea.fr/science_en_ligne/carte_potentiels_microscopiques/carte_potentiel_nucleaire.htm (2006)
[15] S. Raman, C.W. Nestor JR., P. Tikkanen, *At. Dat Nucl. Dat. Tab.* **78** (2001) 1.
[16] B. Bastin et al., *Phys. Rev. Lett.* **99** (2007) 022503.
[17] M. Stanoiu et al., *Phys. Rev.* **C69**, 034312 (2004)
[18] A. Schiller et al., *Phys. Rev. Lett.* **99** (2007) 112501
[19] Z. Elekes et al., *Phys. Rev. Lett.* **98** (2007) 102502.
[20] P.G. Thirolf et al., *Phys. Lett.* **B485**, 16 (2000)
[21] E. Becheva et al., *Phys. Rev. Lett.* **96** (2006) 012501
[22] C. R. Hoffman et al., *Phys. Rev. Lett.* **100** (2008) 152502

- [23] E. Caurier, ANTOINE code, IReS, Strasbourg 1989-2002
- [24] E. Caurier and F. Nowacki, *Act. Phys. Pol.* **B 30**, 705 (1999).
- [25] F. Nowacki *et al.*, in preparation.
- [26] A. Bohr and B. R. Mottelson, *Nuclear Structure* (Benjamin, New York, 1975), Vol. I
- [27] S. Khan *et al.*, *Phys. Lett.* **B156** (1985) 155.
- [28] E. Khan, N. Sandulescu, M. Grasso, and N. Van Giai, *Phys. Rev.* **C 66** (2002) 024309.
- [29] B.D. Serot and J.D. Walecka, *Adv. Nucl. Phys.* **16** (1986) 1.
- [30] B.D. Serot and J.D. Walecka, *Int. J. Mod. Phys.* **E6** (1997) 515.
- [31] G.A. Lalazissis, J. Konig, and P. Ring, *Phys. Rev.* **C55** (1997) 540.
- [32] G.A. Lalazissis, S. Raman, and P. Ring, *At. Data Nucl. Data Tables* **71** (1999) 1.
- [33] B.G. Todd-Rutel and J. Piekarewicz, *Phys. Rev. Lett.* **95** (2005) 122501.
- [34] G.A. Lalazissis, T. Nikšić, D. Vretenar and P. Ring, *Phys. Rev.* **C 71**, 024312 (2005).
- [35] D. Vretenar, A. V. Afanasjev, G. A. Lalazissis, and P. Ring, *Phys. Rep.* **409**, 101 (2005).
- [36] J. F. Berger, M. Girod, and D. Gogny, *Nucl. Phys.* **A 428**, 23 (1984).
- [37] J. F. Berger, M. Girod, and D. Gogny, *Comp. Phys. Comm.* **63**, 365 (1991).